Optimal Collision Energy for Higgs Precision Measurements at the ILC250

Andrea Siddharta Maria[1,*] and *Junping* Tian[2,**]

[1]École polytechnique de Paris - ETH Zurich
[2]International Center for Elementary Particle Physics (ICEPP/University of Tokyo)

Abstract. In the context of the International Linear Collider, the following research aims to look for the best energies for this machine to work at in order to achieve the most precise measurements on Higgs related quantities. We will firstly focus on the measurement of the Higgsstrahlung cross-section, by carrying out a full model-independent analysis at three different energies, with the aim to minimize the relative error on this quantity. Afterwards, we will set up, in the framework of Effective Field Theories, a toy Lagrangian, and we will study the precision of anomalous couplings measurements at the energy points aforementioned. In order to do this, we will build up a chi-squared function at each energy point and look at their contours. The chi-squared functions we will construct exploit the new Lorentz structures present in our Lagrangian, making use of the different angular distribution predicted by this *beyond the standard model* theory, and in particular of its energy dependence. We will also take linear combinations of the three chi-squared at the various energy points, aiming to improve our measurements by running the ILC at multiple energies in a short energy range.

1 Introduction

In spite of the Standard Model (SM) being an extremely accurate theory, its failure at describing certain aspects of our universe (for instance the abundance of matter over anti-matter) has made necessary a search for new physics ever since the SM was completed in 2012 with the discovery of the Higgs boson [1, 2]. The latter in particular is one of the most singular particles in the SM and is the one with the highest potential of hiding Beyond the Standard Model (BSM) physics [3]. To answer this question though a much higher precision of our current Higgs related measurements are required, leading to the birth of Higgs factories, among which the ILC certainly represents one of the most mature ones [4]. In this paper, we aim to improve the precision of the machine by proposing alternative beam energies close to the current point of 250 GeV. Specifically, we will analyze three energy points:

240 GeV **250 GeV** **260 GeV**

and we will try to minimize the error on:

- The *Higgsstrahlung cross-section*, to be obtained through a model independent approach,

*e-mail: andmaria@ethz.ch
**e-mail: tian@icepp.s.u-tokyo.ac.jp

- The *anomalous couplings* of the ZZH vertex.

As for the anomalous couplings study, we will pose ourselves in the framework of Standard Model Effective Field Theory (SMEFT), and we will set up an effective Lagrangian:

$$\mathcal{L}_{ZZH} = M_Z^2(\frac{1}{v} + \frac{a}{\Lambda})Z_\mu Z^\mu h + \frac{b}{2\Lambda}Z_{\mu\nu}Z^{\mu\nu}h + \frac{\tilde{b}}{2\Lambda}Z_{\mu\nu}\tilde{Z}^{\mu\nu}h \tag{1}$$

We will only focus on the study of the two anomalous couplings a and b, not taking into account the CP-odd component $\tilde{b}$. Looking at the contours of chi-squared functions built at each energy point will allow us to minimize the uncertainty on the measurements. By smartly combining these chi-squared, we will propose new scenarios where the collider would run at a few energies in a short energy range.

For the following, an integrated luminosity of $L \sim 2000 fb^{-1}$ is assumed to be accumulated using the beam configuration $(P_{e^-}, P_{e^+}) = (-0.8, 0.3)$. The detector we will refer to is the International Large Detector (ILD) [5].

2 Cross-Section Analysis

In this section, we are going to discuss the Higgsstrahlung cross-section analysis at the three different energy points. In the following we will only consider tree-level diagrams. Around 250 GeV, three main processes compete for the Higgs production, namely the ZZ fusion, the WW fusion and the Higgsstrahlung, whose Feynman diagrams are shown in Fig. 1

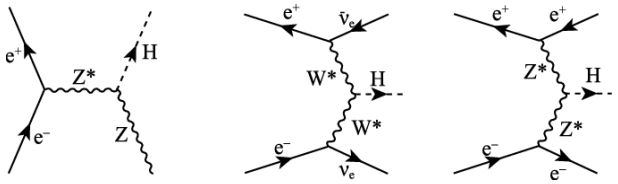

Figure 1. Feynman diagrams of the three main Higgs production process at the ILC250. On the left: Higgsstrahlung. In the center: WW fusion. On the right: ZZ fusion.

As we just want to focus on the Higgsstrahlung process, we can chose an appropriate signal, so as to kill the WW and ZZ fusion. We chose the process:

$$e^+e^- \longrightarrow \mu^-\mu^+h$$

which rules out the other two major processes due to leptonic flavor conservation. This process is almost solely associated to a Higgsstrahlung process where the Z boson further decays into a muonic pair. Another advantage of choosing this process is the very clear experimental trace left by muons, which typically have minimal interaction in the detector and are the only visible particle reaching the outer yoke[6]. In Fig. 3 the behavior of the signal cross-section is shown when considering just ISR or including beamsstrahlung as well.

The background is mostly composed of processes with an even amount of fermions, due to the initial barionic and leptonic numbers being null. The notation we will use for addressing background will comprise of the amount of fermions in the final state (regardless of any boson that might be generated) and of their type: leptonic (if all the fermions in the final state are only leptons), hadronic (in case the fermions in the final state are only hadrons) and semileptonic (for configurations comprising of both hadrons and leptons in the final state).

Our background will therefore be noted as 2f_l (final state comprising of two leptons), 4f_sl (final state formed by two leptons and two hadrons) or 6f_h (six hadrons in the final state). Notice that as processes with a higher amount of fermions in the final state are less probable, so that in the following we will just focus on the 2f, 4f background.

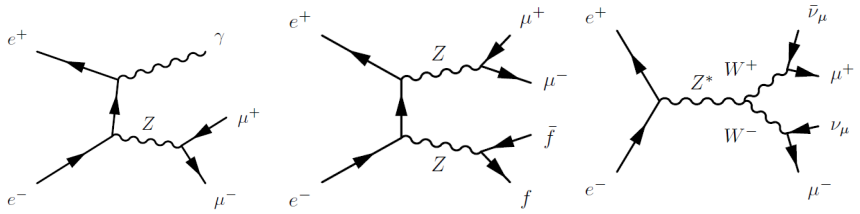

Figure 2. Feynman diagrams for the 3 main background processes. The one on the left is a 2f_l, the central one would be a 4f_sl or 4f_l according to whether the fermions would be a pair of hadrons or leptons and the one on the right finally is a 4f_l process.

The common Monte-Carlo sample for ILD mc-2020 was used for the background and signal at 250 GeV. The signal events for 240/260 GeV are generated by Whizard [7], and then simulated and reconstructed using ILCSoft [8]. The background at all three energy points was assumed to be the same as at 250 GeV.

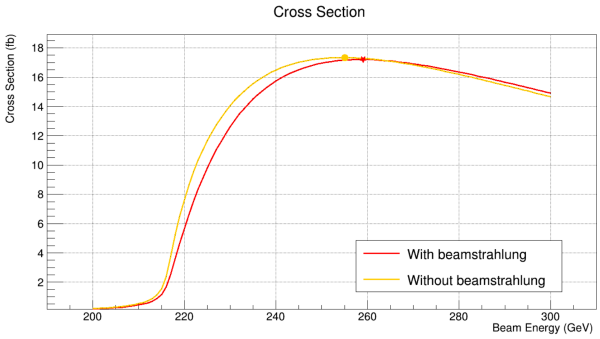

Figure 3. Signal Cross-Section between 200 and 300 GeV at the ILC considering only ISR and including beamsstrahlung as well for a $e_L^- e_R^+$ collision, which is the dominant one in the beam configuration $(-0.8, 0.3)$ we are considering. For both functions, the peak is marked, and lies at higher energies.

As we aim to study the Higgsstrahlung process in a model independent approach, we are going to use the recoil mass technique[9], which requires us to only focus on the di-lepton system stemming from the Z boson decay. To do this, we define the recoiling mass as:

$$M^2_{rec} = (\sqrt{s} - E_{\mu^+\mu^-})^2 - |\vec{p}_{\mu^+\mu^-}|^2 \tag{2}$$

where $E_{\mu^+\mu^-}$ stems for the energy of the di-lepton system, and $\vec{p}_{\mu^+\mu^-}$ represents the sum of the two leptons' momenta. The Higgsstrahlung cross-section is proportional to the amount of signal events, following:

$$\sigma_{ZH} = \frac{N_S}{BR(Z \to \mu^+\mu^-)\varepsilon_S L} \tag{3}$$

so that the quantities we are required to find out are the total amount of signal events N_S and the efficiency of the signal process ε_S. When looking for signal events we are required to

find an appropriate muonic pair. To achieve this, we introduce an algorithm we are going to refer to as the *lepton finder*[10]. The Z boson decays into two *isolated* leptons, meaning they should not belong to any hadronic jet. To look for isolated leptons we are first going to use some (pre)cuts, which can differ on whether the detected particle might be a muon or an electron:

- $p_{track} > 5GeV$: the momentum of the generated leptons right after the collision (and hence in the tracker) should be quite high, given the high mass difference between the Z boson and $l^{\pm}$,
- $[\mu^{\pm}]\, E_{CAL,tot}/p_{track} < 0.3$: if the lepton we are looking at is a muon or an anti-muon, it should have lost very little of its energy in the calorimeters; as we said earlier, they tend to not interact in the detector and typically deposit most of their energy in the outer yoke,
- $[e^{\pm}]\, 0.5 < \frac{E_{CAL,tot}}{p_{track}} < 1.3$: on the other hand electrons and positrons are mostly annihilated in the ECAL, so we require most of their momentum to be absorbed in the calorimeters,
- $[\mu^{\pm}]\, E_{yoke}$ >1.2 GeV: most energetic muons, such as the ones generated by the Z decay, should annihilate in the iron yoke, so that the energy deposited in the yoke should be non null,
- $[e^{\pm}]\, \frac{E_{ECAL}}{E_{CAL,tot}} > 0.9$: most of the energy lost in the calorimeter for an electron is absorbed in the ECAL,
- $[\mu^{\pm}]\, |\frac{d_0}{\delta d_0}| < 5$: the mouns should be generated close to the interaction point. d_0 represents the transversal impact parameter, whereas δd_0 is the uncertainty on this measurement,
- $[e^{\pm}]|\frac{d_0}{\delta d_0}| < 50$: electron uncertainty on the transversal impact parameter is typically lower than for muons,
- $|\frac{z_0}{\delta z_0}| < 5$ where z_0 represents the longitudinal impact parameter.

Once these precuts are applied, we look at the neighboring particles in a cone by using a neural network, so as to make sure the leptons are indeed isolated. After this, we might end up with no isolated lepton (indicating that neither the Z nor the Higgs decayed into a leptonic pair) or on the other hand we might find several isolated leptons. To guard the model independence of our measurements it is required for the muonic pair to not come from the Higgs decay. To ensure this, every possible letpon-antilepton pair of the same flavor is checked, and the one minimizing the following chi-squared function is chosen:

$$\chi^2(m_Z, M_{rec}) = \frac{(m_Z - M_Z)^2}{\sigma^2_{m_Z}} + \frac{(M_{rec} - M_H)^2}{\sigma^2_{M_{rec}}} \tag{4}$$

where m_Z would be the invariant mass of the di-lepton system, which should be as close as possible to the mass of the Z boson M_Z; M_H is the Higgs boson mass, whereas $\sigma^2_{m_Z}$ and $\sigma^2_{M_{rec}}$ are the standard deviations, determined by a Gaussian fit to the distributions of m_Z and M_{rec}; $M_H \sim 125$ GeV is the Higgs boson mass value. To suppress the background, we have introduced the following cuts on kinematical variables:

- $l^{\pm} = \mu^{\pm}$: we require the lepton pair found by the lepton finder to be a $\mu^+\mu^-$ pair,
- $m_Z \in (84, 100)$ GeV: We require a quite tight cut on the invariant mass of the di-muon system (this helps reduce the leptonic backgrounds, especially the 4 fermion ones),
- $E_{vis} > 10$ GeV: The observed energy deposited in the detector should be higher than 10 GeV. This cut is useful for decreasing the influence of leptonic 2f_l, 4f_l comprising of neutrinos, which are undetectable,

- $|\cos(\theta_{mis})| < 0.975$: this cut allows us to suppress greatly the leptonic and semi-leptonic background, which mostly arise from radiative return processes,
- $m_{rec} \in (110, 155)$ GeV: We only want to focus on a region close to the Higgs mass peak.

we chose these cuts so as to maximize the *significance*, defined as follows:

$$\mathcal{S} = \frac{N_S}{\sqrt{N_S + N_B}} = \frac{N_S}{\sqrt{N}} \tag{5}$$

which, in the assumption of Poissonian distribution, would give us a hint of the behavior of the inverse of the relative error. The cut table for the 250 GeV energy point is shown in Table 1, where the efficiency of the signal $\varepsilon = \frac{N_{after\ cuts}}{N_{before\ cuts}}$ is also reported.

Table 1. Cut table for the 250 GeV energy point. The amount of events are normalized to 2000 fb^{-1}.

Cut	N_S	ε	$\mathcal{S}$	2f_l	2f_h	4f_l	4f_sl	4f_h	N_B
No cuts	20616	100%	9.4	$2.6 \cdot 10^7$	$1.55 \cdot 10^8$	$2.08 \cdot 10^7$	$3.83 \cdot 10^7$	$3.36 \cdot 10^7$	$2.73 \cdot 10^8$
Lepton finder	19429	94.2%	9.2	$1.46 \cdot 10^6$	5338	$2.18 \cdot 10^6$	824257	271	$4.47 \cdot 10^6$
$l^+l^- = \mu^+\mu^-$	19419	94.2%	13.9	$1.41 \cdot 10^6$	43.21	325287	209695	2.15	$1.95 \cdot 10^6$
$m_Z \in (84, 100)$ GeV	17425	84.5%	15.5	$1.02 \cdot 10^6$	8.25	76712	157181	0.72	$1.25 \cdot 10^6$
$E_{vis} > 10$ GeV	17418	84.5%	16.7	841930	8.25	68265	157181	0.72	$1.07 \cdot 10^6$
$\|\cos(\theta_{mis})\| < 0.975$	15672	76%	23	290219	5.75	35940	123119	0.48	449284
$m_{recoil} \in (110, 155)$ GeV	15579	75.5%	66	9616	1.45	10493	19954	0.48	40066

Due to the small energy range we are dealing with, two assumptions were made:

- The same cuts were made at all the three energy points, assuming the value of significance with these cuts to be about the same when applying optimal cuts
- The background is assumed to not change with energy

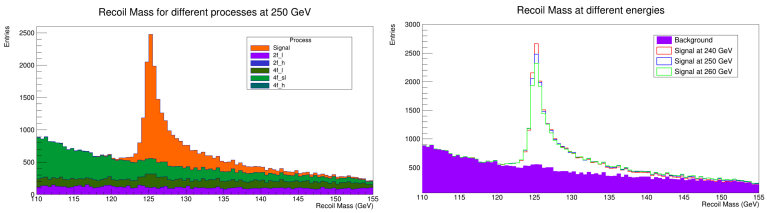

Figure 4. On the left: Recoil Mass distribution at 250 GeV after cuts. On the right: Recoil Mass distribution at all three energy points.

The relative error at all three energy points was evaluated in the assumption of independent binning by applying the following:

$$\frac{\Delta\sigma}{\bar{\sigma}} = \frac{1}{\sqrt{\sum_{i=1}^{nbin} \mathcal{S}_i^2}} \tag{6}$$

where the single $\mathcal{S}_i$ are the significances of the single bins. In Fig. 4, the recoil mass distribution for 250 GeV is shown on the left, whereas a comparison between all three energy points is displayed on the right hand side. The relative statistical precision of the Higgsstrahlung cross-section we found:

	240 GeV	250 GeV	260 GeV
$\frac{\Delta\sigma}{\bar{\sigma}}$	1.11%	1.11%	1.14%

The relative errors at the three energy points is basically the same, the higher energy having slightly lower resolution due to radiative energy losses as we have seen earlier. The result on the 250 GeV energy point can be compared with some previous studies carried out on the same sample[11].

3 Anomalous Couplings

The anomalous couplings of the ZZH vertex were studied in the context of SMEFT by introducing the following the following Lagrangian:

$$\mathcal{L}_{ZZH} = M_Z^2(\frac{1}{v} + \frac{a}{\Lambda})Z_\mu Z^\mu h + \frac{b}{2\Lambda}Z_{\mu\nu}Z^{\mu\nu}h + \frac{\tilde{b}}{2\Lambda}Z_{\mu\nu}\tilde{Z}^{\mu\nu}h \tag{7}$$

where:

- M_Z is the Z boson's mass,
- $v \sim 246$ GeV is the Higgs boson vacuum expectation value,
- $\Lambda \sim 1000$ GeV is the energy scale associated with the new physics; we set it to 1000 GeV as a reference,
- a is a BSM parameter acting as an additional prefactor for the SM component of the ZZH vertex. This anomalous coupling rescales the SM Lagrangian, and hence the cross-section, *without affecting its shape*,
- $Z_{\mu\nu} = \partial_\mu Z_\nu - \partial_\nu Z_\mu$ is the Z boson's strength tensor. This introduces a new Lorentz structure in the ZZH vertex, which affects cross-section shape and the angular distribution of events. It is very important to notice that because of the partial derivation in this component, our Lagrangian itself is now **energy dependent**,
- $\tilde{Z}_{\mu\nu} = \epsilon_{\mu\nu\sigma\rho}Z^{\sigma\rho}$ is the dual tensor of the Z boson,
- The anomalous coupling b is the CP-even coupling between the Higgs scalar and the Z boson at mass-dimension 5,
- The anomalous coupling $\tilde{b}$ is the CP-odd coupling between the Higgs scalar and the Z boson at mass-dimension 5.

The total cross-section arising from this Lagrangian is supposed to be a quadratic form in both a and b. Both these two parameters affect total cross-section, so that by exclusively studying this quantity, we would not be able to probe them both independently. In order to experimentally study both these parameters, we can exploit the new Lorentz structure, which affects angular distribution shape as well as total cross-section. There is different angular variables we can use for this purpose; in the following we are going to use the Z production angle, defined as the angle between the longitudinal direction, defined as the line along which the colliding leptons are moving, and the the Z momentum, which is obtained by summing the momenta of the muon and anti-muon.

The method we used was based on the construction at each energy point of the following chi-squared function:

$$\chi^2 = \sum_{i=1}^{nbin}\left[\frac{N_{SM}\varepsilon_i\frac{1}{\sigma_{SM}}\frac{d\sigma_{SM}}{dx}(x_i) - N_{BSM}\varepsilon_i\frac{1}{\sigma_{BSM}}\frac{d\sigma_{BSM}}{dx}(x_i;a,b)}{\Delta\sigma(x_i)}\right]^2 + \left[\frac{\sigma_{SM} - \sigma_{BSM}(a,b)}{\delta\sigma\cdot\sigma_{SM}}\right]^2 = \chi^2_{shape} + \chi^2_{total} \tag{8}$$

We have separated the chi-squared functions into contributions from the shape and from total cross-section. The reason we want to do this involves how they affect the correlation between a and b. In this chi-squared:

- We have taken the differential cross-section profiles and we decompose them into histograms. The summation runs over all the bins composing these histograms. The histograms are taken as a function of $cos(\theta_Z)$: the cosine of the Z boson's production angle with respect to the longitudinal axis,
- σ_{SM} is the total cross-section predicted by the Standard Model,
- $\sigma_{BSM}(a, b)$ is the total cross-section as predicted by our toy model. Its value changes according the values of a and b,
- $\delta\sigma_{SM}$ is the relative error we experimentally find when measuring our cross-section,
- $\Delta\sigma(x_i)$ is the standard deviation associated with the specific bin. For each bin in the differential cross-section histogram, we have plotted the associated recoil mass distribution and evaluated its error by applying Eq. 6,
- N_{SM} is the amount of events as predicted by the SM (namely $\sigma_{SM} \cdot L$),
- N_{BSM} is the amount of events as predicted by the BSM theory $\sigma_{BSM} \cdot L$,
- $\frac{1}{\sigma}\frac{d\sigma}{dx}$ represent the **normalized** differential cross-section for SM and BSM case. We want to normalize it so as to decouple the shape contribution and the total cross-section contribution,
- $\varepsilon_i = (\frac{N_{after\ cuts}}{N_{before\ cuts}})_i$ is the bin-by-bin efficiency of the signal, it basically represents the sensitivity our detector has in a specific direction. We obtained these values by taking the ratio of signal events before and after cuts. Other than those cuts, we have introduced a new cut requiring at least 3 particles in the Higgs decay. This cut works on a parameter related to jet shower reconstruction and it helps us suppress the semileptonic background. As it affects the efficiency of different Higgs decay modes we could have not used it during our cross-section analysis, because it would have compromised the model independence, given that most of the Higgs branching ratio comes from hadronic decays (mostly to $b\bar{b}$). Because the differential cross-section does not depend on Higgs decay, adding this cut does not compromise our analysis strategy.

We are going to use these chi-squared function by looking at the contours $\chi^2 = 1$, which contain 68% of the total probability mass distribution and are therefore the region in the (a, b) plane where the true values of these parameters are most likely going to lie.

The χ^2_{shape} contribution has a quite low correlation, whereas χ^2_{total} is highly correlated. As the contribution from the shape increases with energy due to the newly introduced Lorentz structure, the correlation is going to diminish with energy, making our measurements more precise.

In order to constraint even more our measurements, we can go even further. We can exploit the correlation at lower energies to achieve high precision measurements. Take a look at Fig. 5. Imagine we generate a contour at a certain energy E_{low} (in blue in the figure). After this we raise the energy of our collider to a higher energy $E_{high} > E_{low}$ and we look at its contour (drawn in orange in the picture). Due to the decrease in correlation, this new contour is going to be slightly tilted compared to the other one, tending to look more like an ellipse disposed along the axis. Now, because (a, b) do not depend on energy, their true values will have to lie in the intersecting area, leading to a much tighter constraint of these two parameter!

We can actually do more than just looking at the intersection area. We can build up a new chi-squared function as a sum of the chi-squared at different energies. The region $\chi^2_{low} + \chi^2_{high} < 1$ is shown in Fig. 5 as a green area; you might notice it's slightly smaller than the intersection area. This happens because the singular chi-squared are non-negative

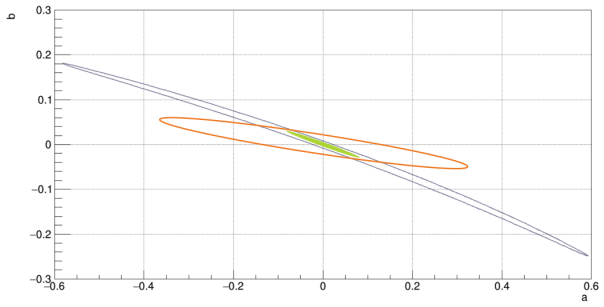

Figure 5. Hypothetical contours at two different energies. The blue colored contour would correspond to the energy E_{low} and the orange one to E_{high}. The green area is the zone where most likely the real value of our parameters will lie.

functions. Take for instance the intersection points: the value of the cumulative chi-square here is of 2, so that they will necessarily lie further away from the contour $\chi^2_{low} + \chi^2_{high} = 1$.

In the most general case we can take a linear combination of these functions, so that we would end up with:

$$\chi^2 = c_{240}\chi^2_{240} + c_{250}\chi^2_{250} + c_{260}\chi^2_{260} \tag{9}$$

The physical meaning of these c_E is sharply outlined. Each c_E represent the fraction of total (integrated) luminosity that we need to accumulate at each energy point, so that for n energy points it follows the physical constraint

$$\sum_{i=1}^{n} c_{E_i} = 1 \quad ; \quad 0 \leq c_{E_i} \leq 1 \tag{10}$$

The final question we are then asking ourselves is: *How much luminosity should we accumulate at each energy point to obtain the best measurements of anomalous couplings?*

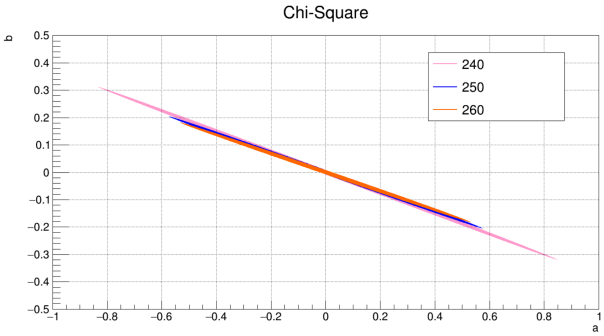

Figure 6. Chi-Squared contours at the three energy points, expressed in GeV.

In Fig. 6 the contours at the three different energy points are shown. The results are summerized in Table 2.

The uncertainties on anomalous couplings can be improved by about about 32% by using an appropriate combination of the three energy points! We should not be surprised that the

Table 2. In this table, the results for different quantities are resumed for different configuration. The last column exposes the configuration that minimizes a specific quantity and the second-to-last column gives us the value of that quantity at the best configuration.

	χ^2_{240}	χ^2_{250}	χ^2_{260}	**Best**	$(c_{240}, c_{250}, c_{260})$
Correlation	-0.9993	-0.9984	-0.9981	-0.9965	(0.4,0,0.6)
$2\Delta a$	1.681	1.149	1.067	0.776	(0.5,0,0.5)
$2\Delta b$	0.631	0.410	0.365	0.276	(0.4,0,0.6)
Area	0.02236	0.01477	0.01334	0.0098	(0.4,0,0.6)

combination that improves the most our measurements is $(c_{240}, c_{250}, c_{260}) = (0.4, 0, 0.6)$. The precision of our measurements is tightly linked to the intersecting area between the different contours. As between the two energy points at 240 GeV and 260 GeV the highest relative tilt is present, the intersecting area is minimized when considering only these two values, as shown in both Table 2 and Fig. 6. We notice how the uncertainties on a and b are minimized by two slightly different configurations. This happens because the contours tend to tilt counterclockwise as energy rises, with the major axis of the ellipse disposed along the a-axis; a configuration with a lower contribution from higher energy would then benefit the measurement on a.

Other than this general case, we have also imagined a scenario where only the lower energy points 240 GeV and 250 GeV would be available. The results in this case are exposed in Table 3

Table 3. Results obtained for the quantities of interest when considering just the 240 GeV and 250 GeV energy points.

	χ^2_{240}	χ^2_{250}	**Best**	(c_{240}, c_{250})
Correlation	-0.9993	-0.9984	-0.9981	(0.4,0.6)
$2\Delta a$	1.681	1.149	1.042	(0.4,0.6)
$2\Delta b$	0.631	0.410	0.378	(0.3,0.7)
Area	0.02236	0.01477	0.013437	(0.4,0.6)

Here, the improvement margin is much smaller of about 7%, but still proves the validity of the method used here and its usefulness: by *decreasing* our beam energy and combining data in a smart way, we are actually able to provide much more precise results!

In both cases, the area is minimized by the same configuration that minimizes the correlation, which also happens to be extremely close to most precise configuration possible.

It's interesting to point out that in spite of this research being carried out in the context of the ILC250 and using a specific Lagrangian, this contour method we applied here is actually quite general and could potentially be used in several colliders, and applied to a vast set of theories.

4 Summary

The ILC250 is supposed to work at 250 GeV, based on the theoretical peak of the Higgsstrahlung process. In spite of this, when considering the collision of real beams comprehensive of all the satellite phenomena that can take place at a linear collider, this energy does not necessarily provide us with the most accurate measurements, but leads to a precision comparable with other energy points in a 10 GeV range. On the other hand, the EFT theory

we have set up during in the latter part shows a great improvement when taking our measurements at different energies in a short range, suggesting probing new physics could actually be much easier when considering a few energy point in a short range, instead of fixing ourselves on a singular center of mass energy.

References

[1] G. Aad et al., ATLAS Collaboration, “Observation of a new particle in the search for the Standard Model Higgs boson with the ATLAS detector at the LHC”, Phys. Lett. B 716 (2012)

[2] S. Chatrchyan et al., CMS Collaboration, “Observation of a new boson at a mass of 125 GeV with the CMS experiment at the LHC”, Phys. Lett. B 716 (2012)

[3] L.Wang et al.,"A Concise Review on Some Higgs-Related New Physics Models in Light of Current Experiments", Universe 9 (2023)

[4] J.Tian et al., "ILC White Paper", Proceedings, 2013 Community Summer Study on the Future of U.S. Particle Physics: Snowmass on the Mississippi (CSS2013)

[5] Ties Behnke et al., “The International Linear Collider Technical Design Report- Volume 4: Detectors”, arXiv:1306.6329 [hep-ex]

[6] V.Boudry et al., "Lepton identification at particle flow oriented detector for the future e^+e^- Higgs factories",Eur.Phys.J.C 77 (2017)

[7] Wolfgang Kilian, Thorsten Ohl, and Jurgen Reuter, “WHIZARD: Simulating Multi-Particle Processes at LHC and ILC,” Eur. Phys. J. C71, 1742 (2011)

[8] "ILCSoft Home Page":"https://ilcsoft.desy.de/portal"

[9] H.Li,"Higgs Recoil Mass and Higgs-Strahlung Cross-Section Study for the ILD LOI", Contribution to LCWS10 and ILC10

[10] Junping Tian, “Isolated lepton tagging and new jet clustering,” the 43 General Meeting of ILC PhysicsSubgroup (2015), KEK.

[11] J.Tian et al.,"Measurement of the Higgs boson mass and $e^+e^- \to ZH$ cross section using $Z \to \mu^+\mu^-$ and $Z \to e^+e^-$ at the ILC", Phys.Rev.D 94 (2016) 11, 113002, Phys.Rev.D 103 (2021) 9, 099903 (erratum)